Identification of Lennard–Jones potential parameters from concentration distributions using machine learning*

Igor Boyko[1,*†], Julia Seti[2,†], Oksana Bahrii-Zaiats[3,†], Oksana Petryk[1,†]

[1] Ternopil Ivan Puluj National Technical University, Rus'ka St, 56, Ternopil, 46001, Ukraine
[2] Lviv Polytechnic National University, Stepan Bandera St, 12, Lviv, 79013, Ukraine
[3] I. Horbachevsky Ternopil National Medical University, Maidan Voli St., 1, Ternopil, 46002, Ukraine

Abstract

A consistent methodology of the approach is proposed, which allows establishing the parameters of the Lennard–Jones potential for diffusion processes in mesoscale materials in the quantum-mechanical description of the activation energies of the phase transition. The developed method is based on the regression of data obtained by analyzing concentration distribution data and applying the machine learning method of the convolutional neural network. The proposed method allows establishing the parameters of the Lennard–Jones potential with reliable accuracy directly from the specified spatial concentration distributions and determining the substance to which these parameters correspond.

Software implementation of data regression and machine learning of the neural network was carried out using specialized Python libraries, namely: Scikit-learn, TensorFlow, and PyTorch. The obtained results and the developed method will be useful for specialists in the field of physical chemistry and nanomaterials science.

Keywords

Lennard–Jones potential, mesoscale materials, diffusion processes, machine learning

1. Introduction

Nanoscale and mesoscopic materials [1-4] are of significant practical interest for modern technologies. They are composite devices operating in various areas of electronics, physical and chemical technology, crystallography, and the development of new functional materials and compounds [5-7]. This is primarily due to the wide selection of existing materials from which a variety of nano- and micro-scale structures can be created. For this purpose, metals, semiconductors, organic semiconductors, and various magnetic materials can be used.

One of the main directions concerning the use and research of mesoscopic materials is to increase their efficiency in practical applications and to ensure the achievement of stability of this work. This problem has a fairly broad nature and a variety of its manifestations, and in general it cannot be solved by a simple experimental or theoretical study of these materials, in particular by mathematical modeling of their properties and precision characteristics, but requires a broader and more detailed analysis.

Examples of such low-density structures are materials with micropores — the so-called zeolites, which are widely used both in catalytic processes and in electronics. The properties of these mesostructures in their kinetics are mainly determined by the energies of molecular transitions or so-called activation energies corresponding to molecules of volatile hydrocarbons or charged microparticles. At the same time, these energies depend significantly on the size of these particles and the properties of interaction in the environment of these mentioned materials. As a result, the

* The 5th International Conference on Information Technologies: Theoretical and Applied Problems| (ITTAP-2025) October 22-24, 2025 Ternopil, Ukraine, Opole, Poland
[1*] Corresponding author.
[†] These authors contributed equally.
boyko.i.v.theory@gmail.com (I. Boyko); jseti18@gmail.com (Ju. Seti); bagrijzayats@tdmu.edu.ua (O. Bahrii-Zaiats); oopp3@ukr.net (O. Petryk)
0000-0003-2787-1845 (I. Boyko); 0000-0001-5576-8031 (Ju. Seti); 0000-0002-5533-3561 (O. Bahrii-Zaiats); 0000-0001-8622-4344 (O. Petryk);

construction of even microscopic models of such physical processes does not allow to fully identify the parameters of the kinetics of microparticles in cellular materials due to a fairly wide spread of their geometric parameters. Such a problem requires the use of additional methods, in particular, the analysis of a large number of concentration distributions together with the calculation of the activation energy and the subsequent application of information technology tools. Such methods can be machine learning methods and convolutional neural networks, which allow to systematize the obtained results and adequately identify material parameters in various materials with a porous structure.

2. Microscopic model of activation energies of methane and propane in porous materials, kinetics of microparticles

We begin by considering a sample of a porous material that has a spherical shape of radius R and contains pores with an average radius $\bar{r}=r$. The geometric structure of such a sample and an separate micropore is shown in Fig 1.

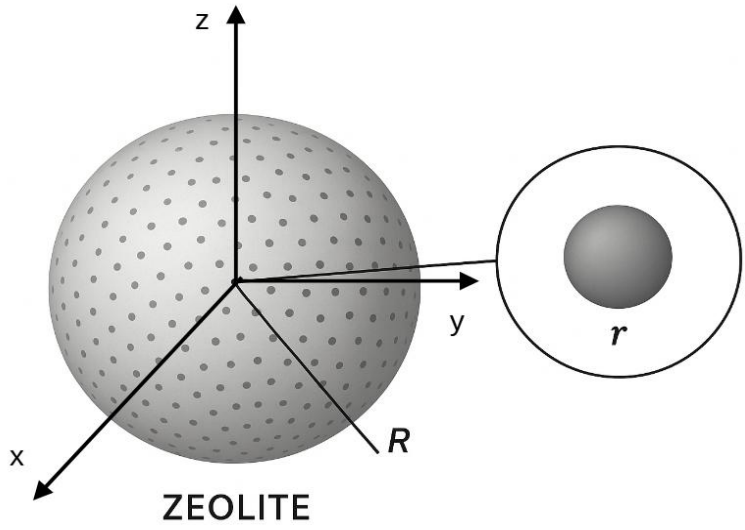

Figure 1: Geometric diagram of a porous sample of spherical shape with a micropore contained in it.

It is assumed that inside each micropore a particle (in our case, methane or propane molecules) interacts with the sample material. This interaction is described by the Lennard-Jones potential. Thus, the molecule falls into a potential trap, the geometric dependence of which $U=U(r)$ in the selected coordinate system can be represented as follows:

$$U(r)=4\epsilon[(\sigma/r)^{12}-(\sigma/r)^{6}], \tag{1}$$

where in our case r is the distance from the center of the molecule to the center of time localizing this molecule. The values ϵ and σ characterize, respectively, the depth of the potential well of the micropore and the distance at which $U(\sigma)=0$.

Since in our problem we are dealing with hydrocarbon molecules, it is impossible to apply formula (1) directly. It should be taken into account that according to the principles of quantum chemistry, the wave functions of molecules such as methane (CH_4) and propane (C_3H_8) can be constructed from the atomic orbitals of carbon and hydrogen. In the case of methane, sp^3 hybridization occurs, as a result of which, in the wave function, the sp^3 hybrid orbitals of carbon will overlap with the 1s orbitals of all four carbon atoms. This leads to the wave function of the methane molecule in the following form:

$$\psi_{CH_4}(r)=\frac{1}{2}\sum_{i=1}^{4}\left(\psi_{2s}(r)+d_i\cdot(\psi_{2p_x}(r),\psi_{2p_y}(r),\psi_{2p_z}(r))\right) \tag{2}$$

where $d_i=(\pm1;\pm1;\pm1)$ - this is a vector that specifies the direction of the hybrid orbital and takes into account all four possible directions realized by combinations of signs. The functions directly sought look like as follows:

$$\begin{aligned}
\psi_1(r)&=\frac{1}{2}(\psi_{2s}(r)+\psi_{2p_x}(x,y,z)+\psi_{2p_y}(x,y,z)+\psi_{2p_z}(x,y,z))\\
\psi_2(r)&=\frac{1}{2}(\psi_{2s}(r)+\psi_{2p_x}(x,y,z)-\psi_{2p_y}(x,y,z)-\psi_{2p_z}(x,y,z))\\
\psi_3(r)&=\frac{1}{2}(\psi_{2s}(r)-\psi_{2p_x}(x,y,z)+\psi_{2p_y}(x,y,z)-\psi_{2p_z}(x,y,z))\\
\psi_4(r)&=\frac{1}{2}(\psi_{2s}(r)-\psi_{2p_x}(x,y,z)-\psi_{2p_y}(x,y,z)+\psi_{2p_z}(x,y,z)).
\end{aligned} \tag{3}$$

The explicit form of the functions $\psi_{2s}(r),\psi_{2p_x}(r),\psi_{2p_y}(r),\psi_{2p_z}(r)$is as follows:

$$\begin{aligned}
\psi_{2s}(r)&=\frac{1}{4\sqrt{2\pi a_B^3}}\left(2-\frac{r}{a_B}\right)e^{-r/(2a_B)}\\
\psi_{2p_x}(x,y,z)&=\frac{1}{4\sqrt{2\pi a_B^5}}x\,e^{-\sqrt{x^2+y^2+z^2}/(2a_B)}\\
\psi_{2p_y}(x,y,z)&=\frac{1}{4\sqrt{2\pi a_B^5}}y\,e^{-\sqrt{x^2+y^2+z^2}/(2a_B)}\\
\psi_{2p_z}(x,y,z)&=\frac{1}{4\sqrt{2\pi a_B^5}}z\,e^{-\sqrt{x^2+y^2+z^2}/(2a_B)}
\end{aligned} \tag{4}$$

where a_B - is the Bohr radius.

In the case of propane, we will have a chain of three carbon atoms in sp^3 hybridization with four sp^3 orbitals. For a single carbon atom (shifted to a point with coordinates (x_C,y_C,z_C)) in a propane molecule, we can write:

$$\begin{aligned}
\psi_i^{(C)}(x,y,z)=\frac{1}{2}\big(&\psi_{2s}(x-x_C,y-y_C,z-z_C)+d_{i,x}\psi_{2p_x}(x-x_C,y-y_C,z-z_C)\big)\\
&+d_{i,y}\psi_{2p_y}(x-x_C,y-y_C,z-z_C)+d_{i,z}\psi_{2p_z}(x-x_C,y-y_C,z-z_C)
\end{aligned} \tag{5}$$

where $\psi_{2s},\psi_{2p_x},\psi_{2p_y},\psi_{2p_z}$ - atomic orbitals calculated according to the relations (4), $d_{i,x},d_{i,y},d_{i,z}$ - components of direction $d_i=(\pm1;\pm1;\pm1)$, now specifying the orientations of the sp^3 orbital. Now the wave function of the propane molecule can be represented as the sum of all sp^3 orbitals, that is:

$$\psi_{C_3H_8}(x,y,z)=\sum_{C\in C1,C2,C3}\sum_{i=1}^{4}\psi_i^{(C)}(x,y,z) \tag{6}$$

or in a more visual form:

$$\begin{gathered}
\psi_{C_3H_8}(x,y,z)=\sum_{i=1}^{4}\psi_i^{(C1)}(x,y,z)+\sum_{i=1}^{4}\psi_i^{(C2)}(x,y,z)+\sum_{i=1}^{4}\psi_i^{(C3)}(x,y,z)\\
C_1=(-d,0,0),C_2=(0,0,0),C_3=(d,0,0)
\end{gathered} \tag{7}$$

Examples of spatial dependences of wave functions $(|\psi_{CH_4}(x,y,z)|^2, |\psi_{C_3H_8}(x,y,z)|^2)$ corresponding to hybrid sp^3 orbitals for methane and propane molecules are shown in Fig. 2a, b, respectively.

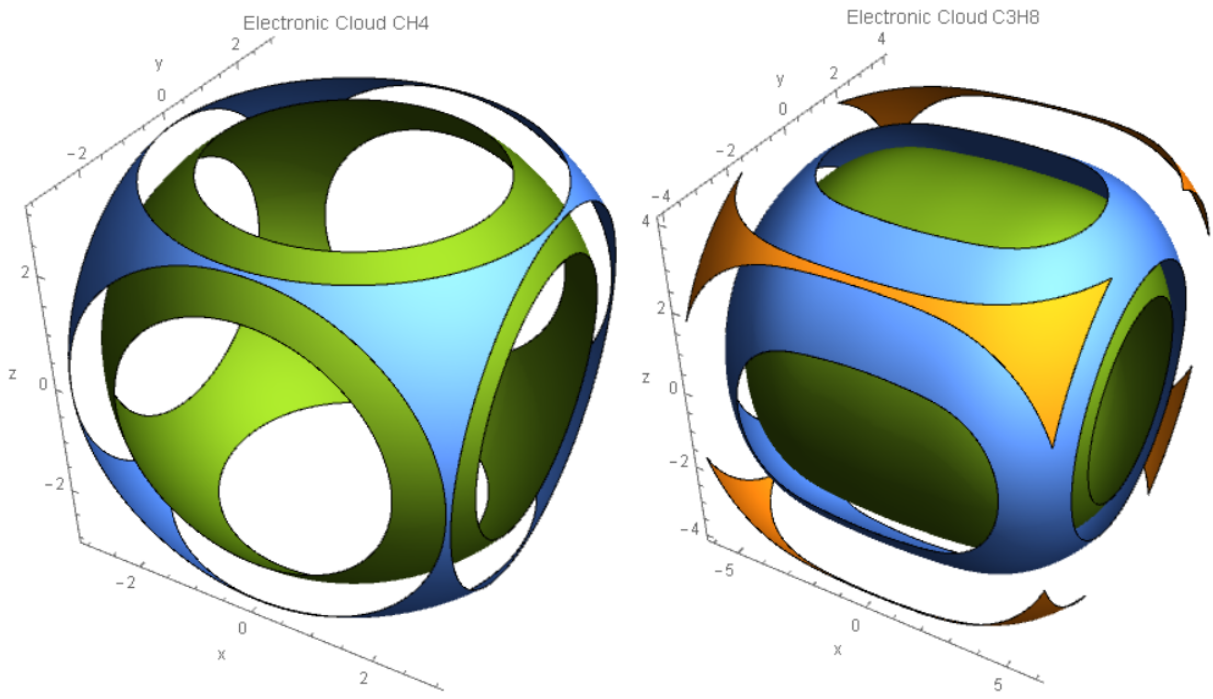

a) *b)*

Figure 2: Squares of the moduli of the wave functions of methane (a) and propane (b) molecules inside a micropore.

Next, we calculated the matrix elements of potential (1) using wave functions (2)-(5), i.e.

$$\widetilde{U_{CH_4}} = 4\epsilon_{CH_4}\langle\psi_{CH_4}(x,y,z)|[(\sigma_{CH_4}/r)^{12}-(\sigma_{CH_4}/r)^{6}]|\psi_{CH_4}(x,y,z)\rangle \quad (8)$$
$$\widetilde{U_{C_3H_8}} = 4\epsilon_{C_3H_8}\langle\psi_{C_3H_8}(x,y,z)|[(\sigma_{C_3H_8}/r)^{12}-(\sigma_{C_3H_8}/r)^{6}]|\psi_{C_3H_8}(x,y,z)\rangle.$$

As a result, the activation energies can be calculated depending on the temperature T as follows:

$$E_{ac}(CH_4) = \widetilde{U_{CH_4}} + \frac{i_{CH_4}}{2}kT\,;\; E_{ac}(C_3H_8) = \widetilde{U_{C_3H_8}} + \frac{i_{C_3H_8}}{2}kT \quad (9)$$

where the number of degrees of freedom for methane and propane, respectively, is: $i_{CH_4}=15\,; i_{C_3H_8}=33.$

3. Automation of methane and propane parameter identification from concentration distributions, and the development and training of a neural network to perform this task

The main objective of our work is to provide automated, high-performance and reliable identification of methane and propane parameters based on a developed mathematical model of activation energy and experimentally obtained concentration distributions. For this purpose, we apply the basic system of kinetic equations inside the material and separately inside the pores. These equations are as follows:

$$\frac{\partial C(r,t)}{\partial t}=D_{eff}\frac{1}{r^2}\frac{\partial}{\partial r}\left(r^2\frac{\partial C(r,t)}{\partial r}\right), \tag{10}$$

$$\frac{\partial q(r,z,t)}{\partial t}=D_p\left(\frac{1}{r}\frac{\partial}{\partial r}\left(r\frac{\partial q(r,z,t)}{\partial r}\right)+\frac{\partial^2 q(r,z,t)}{\partial z^2}\right), \tag{11}$$

together with the Langmuir-type isotherm:

$$q(T)=\frac{q_{max}b(T)C(r,t)}{1+b(T)C(r,t)};b(T)=b_0\cdot\exp(-E_{ac}/RT), \tag{12}$$

where it is taken into account that the dependence on temperature T is determined by the Van 't Hoff law, D_{eff} and D_p - is the diffusion parameters in bulk material and pores.

In order to be able to use the datasets of concentration distributions obtained from experimental measurements, the mathematical model (10)-(12) should be presented in discretized form on a three-dimensional grid:

$$r_i=i\Delta r;z_j=j\Delta z;t^n=n\Delta t; \tag{13}$$

$$C_i^{n+1}=C_i^n+D_{eff}\Delta t\left(C_{i+1}^n-2C_i^n+\frac{C_{i-1}^n}{(\Delta r)^2}+\frac{2}{r_i}C_{i+1}^n-\frac{C_{i-1}^n}{2}\Delta r\right);$$

$$C_0^{n+1}=C_0^n+6D_{eff}\Delta t C_1^n-\frac{C_0^n}{(\Delta r)^2};$$

$$q_{i,j}^{n+1}=q_{i,j}^n+D_p\Delta t\left(q_{i+1,j}^n-2q_{i,j}^n+\frac{q_{i-1,j}^n}{(\Delta r)^2}+\frac{q_{i+1,j}^n}{r_i}-\frac{q_{i-1,j}^n}{2}\Delta r+q_{i,j+1}^n-2q_{i,j}^n+\frac{q_{i,j-1}^n}{(\Delta z)^2}\right);$$

$$q_{0,j}^{n+1}=q_{0,j}^n+D_p\Delta t\left(2q_{1,j}^n-\frac{q_{0,j}^n}{(\Delta r)^2}+q_{0,j+1}^n-2q_{0,j}^n+\frac{q_{0,j-1}^n}{(\Delta z)^2}\right);$$

$$q_{i,j}^{n,(eq)}=b_0\exp(-E_{ac}/RT^n)(1+q_{max})C_i^n.$$

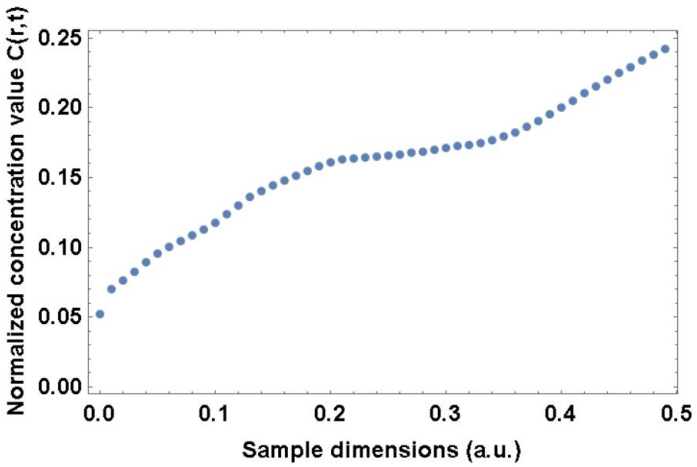

Figure 3: One example of concentration distributions that were used to train a neural network.

Since the parameters ϵ and σ are included in the difference scheme due to the dependence of the activation energy (8) and (9), they can be obtained for each dataset from the last equation (13).

Next, we develop a neural network in which the input is the concentration distributions $C(r,t);q(r,z,t)$ obtained in the experiment (in total, we used 280 datasets taken from works [8-

10] and related ones), and parameters ϵ and σ obtained using finite different scheme (13). An example of a concentration distribution used to train a neural network is shown in Fig. 3.

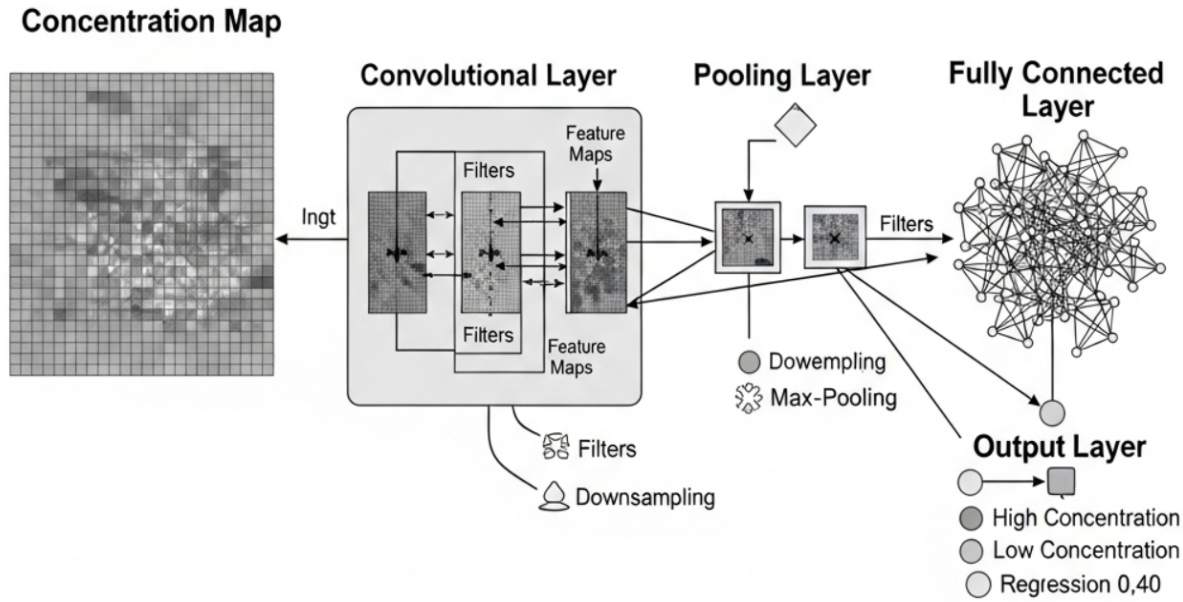

Figure 4: Neural network diagram and its operating principle.

Table 1
Results of the developed neural network for identifying methane and propane parameters from their concentration distributions in different samples. In square brackets next to the number of each sample there is a reference to the work from which the concentration distributions were taken.

Sample number	A substance used as a working agent	Lennard-Jones parameter σ (nm)	Lennard-Jones parameter ϵ(meV)	Prediction (%)
1 [11]	methane	0.370	12.4	98
2 [12]	propane	0.534	20.6	96
3 [13]	propane	0.502	20.4	92
4 [14]	propane	0.571	20.1	95
5 [15]	propane	0.519	20.4	96
6 [16]	methane	0.382	12.9	93

The network was trained using class labels, which were taken to be diffusion coefficients D_{eff}, D_p and parameters ϵ, σ. In this case, the network performs data regression, which ensures a fast and optimal approximation of the numerical solutions of the difference scheme (13). Regression for each difference scheme and class labels produces a stack of maps $C_t \in R^{H \times W}$ for all its nodes. Now the tensor $X \in R^{T \times H \times W}$ is fed into CNNs, which are 3D convolutions over the spatial dimensions with temporal layers as channels over the parameters (t, x, y). The output of the network in the

system is interpreted as an estimate of the set of parameters (D_{eff}, D_p, ϵ, σ), which is the probability of pore morphology classes. The architecture of the developed neural network and an illustration of its operation are presented in Fig. 4. The software implementation of the neural network and work with it was carried out using the Jupiter environment for the Python programming language and the Scikit-learn, TensorFlow, and PyTorch libraries.

The learned neural network was used to identify the parameters of the Lennard-Jones potential and diffusion coefficients based on given input data of concentration distributed in various cellular media. In all text datacenters, concentration distributions were used, for which diffusion processes involving methane or propane occurred. The results of the work of the neural network with concentration distributions taken from experimental works [11-16] are presented in Table 1.

It is accepted that the theoretically calculated values of the Lennard-Jones parameters are equal to $\sigma = 0.373\,nm; \epsilon = 12.7\,meV$ for methane and $\sigma = 0.512\,nm; \epsilon = 20.3\,meV$ for propane, respectively. Table 1 also shows the value of the prediction with which the neural network sets the parameters of the Lennard-Jones potential from the concentration distribution for each of the studied samples. As can be seen from Table 1, the value of prediction is from 92 to 98%. In general, this indicates that the developed neural network allows us to set the parameters of substances used in diffusion of porous samples, namely methane and propane, with sufficiently high accuracy.

4. Conclusions

An approach to identifying the parameters of the Lennard-Jones potential for methane and propane from the concentration distributions of these substances in cellular samples using a trained neural network is proposed. To solve this problem, a microscopic model of the activation energy of methane and propane is used, and a mathematical model of a certain difference scheme is developed based on the equations of diffusion transfer kinetics. The developed neural network is applicable to identifying the parameters of the Lennard-Jones potential in various porous samples. It has been established that the developed method allows determining these parameters with a probability of 92 to 98% only with a concentration distribution at the input. We see the development of the proposed method in its further improvement for application to identifying the parameters of a wider range of volatile hydrocarbons and other substances experimentally studied and technologically applied in porous materials.

Declaration on Generative AI

The authors have not employed any Generative AI tools.

References

[1] R. Coufal, K. Adach, J. Zedník, O. B. Klinovská, S. Petrík, M. Fijalkowski. Fluorescent Nanoporous Materials from Polypropylene-Based Covalent Adaptable Networks, ACS Omega 10 (2025)13954−13965. doi: 10.1021/acsomega.4c10168.

[2] D. Chakraborty, D. Mullangi, C. Chandran, R. Vaidhyanathan. Nanopores of a Covalent Organic Framework: A Customizable Vessel for Organocatalysis, ACS Omega 7 (2022) 15275−15295. doi: 10.1021/acsomega.2c00235.

[3] A. Bachtold, J. Moser, M. I. Dykman. Mesoscopic physics of nanomechanical systems, Reviews of Modern Physics 94 (2022) 045005. doi: 10.1103/RevModPhys.94.045005.

[4] P. Maruschak , I. Konovalenko, A. Sorochak. Methods for evaluating fracture patterns of polycrystalline materials based on the parameter analysis of ductile separation dimples: A reviewMethods for evaluating fracture patterns of polycrystalline materials based on the parameter analysis of ductile separation dimples: A review, Engineering Failure Analysis 153 (2023) 107587. doi: 10.1016/j.engfailanal.2023.107587.

[5] H. Liu, X. Jin, D. Zhou, Q. Yang, L. Li. Potential application of functional micro-nano structures in petroleum, Petroleum Exploration and Development 45 (2018) 745–753. doi: 10.1016/S1876-3804(18)30077-6.

[6] A. S. D. Sandanayaka, T. Matsushima, F. Bencheikh, S. Terakawa, W. J. Potscavage Jr., C. Qin, T. Fujihara, K. Goushi, J.-C. Ribierre, C. Adachi. Indication of current-injection lasing from an organic semiconductor, Applied Physics Express 12 (2019) 061010. doi: 10.7567/1882-0786/ab1b90.

[7] H. Itagaki, Y. Fujiwara, Y. Minowa, Y. Ikehara, T. Kaneko, T. Okazaki, Y. Iizumi, J. Kim, H. Sakakita. Synthesis of endohedral-fullerenes using laser ablation plasma from solid material and vaporized fullerenes, AIP Advances 9 (2019) 075324. doi: 10.1063/1.5100980.

[8] Shuchi Zhang, Dengyun Miao, Yi Ding, Haodi Wang, Tao Peng, Feng Jiao, Xiulian Pan. Size Effect of ZSM-5 on Diffusion and Catalytic Performance in Syngas Conversion to Aromatics over $MnCrO_x$-ZSM-5 Catalyst, The Journal of Physical Chemistry C 129 (2025) 1582–1589. doi: 10.1021/acs.jpcc.4c06565.

[9] Á. López-Martín, A. Caballero, G. Colón. Unraveling the Mo/HZSM-5 Reduction Pre-treatment Effect on Methane Dehydroaromatization Reaction, *Applied Catalysis B: Environmental* 312 (2022) 121382. doi: 10.1016/j.apcatb.2022.121382.

[10] X. Liu, J. Shi, G. Yang, J. Zhou, C. Wang, J. Teng, Y. Wang, Z. Xie. A diffusion anisotropy descriptor links morphology effects of H-ZSM-5 zeolites to their catalytic cracking performance, *Communications Chemistry* 4 (2021) Article 107. doi: 10.1038/s42004-021-00543-w.

[11] Á. López-Martín, M. F. Sini, M. G. Cutrufello, A. Caballero, G. Colón. Characterization of Re-Mo/ZSM-5 catalysts: How Re improves the performance of Mo in the methane dehydroaromatization reaction, Applied Catalysis B: Environmental 304 (2022) 120960. doi: 10.1016/j.apcatb.2021.120960.

[12] K. Bian, S. Liu, J. Zhang, G. Zhang, X. Zhang, G. A. Ocran, M. Wang, Q. Liu, S. Hou, X. Guo. PtFe@S-1 coupling with ZSM-5 for the propane dehydro-aromatization reaction: The effect of acidity and b-axis diffusion distance, Industrial & Engineering Chemistry Research 63 (2024) 20840. doi: 10.1021/acs.iecr.4c03194.

[13] I. B. Dauda, M. Yusuf, S. Gbadamasi, M. Bello, A. Y. Atta, B. O. Aderemi, B. Y. Jibril. Highly selective hierarchical ZnO/ZSM-5 catalysts for propane aromatization, *ACS Omega 5* (2020) 2725–2733. doi: 10.1021/acsomega.9b03343.

[14] Z. Ma, D. Shi, S. Wang, X. Li, Y. Zhang. Control of aluminum distribution in ZSM-5 zeolite for enhancement of its catalytic performance for propane aromatization, Frontiers of Chemical Science and Engineering 18 (2024) 86. doi: 10.1007/s11705-024-2439-8.

[15] P. Zhang, J. Zhuang, J. Yu, Y. Guan, X. Zhu, F. Yang. Disinfectant-assisted preparation of hierarchical ZSM-5 zeolite with excellent catalytic stabilities in propane aromatization, Nanomaterials 14 (2024) 802. doi: 10.3390/nano14090802.

[16] M. Raad, S. Hamieh, J. Toufaily, T. Hamieh, L. Pinard. Propane aromatization on hierarchical Ga/HZSM-5 catalysts, Journal of Catalysis 366 (2018) 223–236. doi: 10.1016/j.jcat.2018.07.035.